

Characterization of thermal modulation of electrical conductivity: a small volume absorbance measurement technique

ROBERT McLAREN AND NORMAN J. DOVICH¹

Department of Chemistry, University of Alberta, Edmonton, Alta., Canada T6G 2G2

Received December 21, 1988

ROBERT McLAREN and NORMAN J. DOVICH. *Can. J. Chem.* **67**, 1178 (1989).

Laser-induced thermal modulation of electrical conductivity is a new photothermal method for the measurement of minute absorbance in sub-nanoliter liquid samples. In this paper, a model is presented for the technique. This model is based upon the interaction of a Gaussian laser beam with a cylindrical, homogeneous electrolytic resistor. Particularly simple results are produced if the laser beam spot size is much smaller than the diameter of the electrodes. The theory is verified with respect to the electrode spacing and to the laser power, spot size, and chopping frequency; the highest sensitivity occurs with low chopping frequency, high laser power, and small electrode spacing. The signal is independent of laser spot size, as long as the beam does not illuminate the electrode surface. The precision of the measurement is dominated by shot noise in the current flow through the electrolytic resistor. One point absorbance detection limits of 5.5×10^{-6} measured across the 76- μm diameter electrode wires are obtained in aqueous solution with a 5-mW helium-neon laser. With this instrument, the difference in the absorbance of water and deuterated water is easily determined at 632.8 nm.

Key words: thermal modulation of electrical conductivity.

ROBERT McLAREN et NORMAN J. DOVICH. *Can. J. Chem.* **67**, 1178 (1989).

La modulation thermique induite au laser de la conductivité électrique est une nouvelle méthode photothermique permettant de mesurer de très faibles absorbances dans des échantillons liquides de volumes plus faibles que le nanolitre. Dans ce travail, on présente un modèle pour cette technique. Ce modèle est basé sur l'interaction d'un faisceau gaussien de laser avec une résistance électrolytique homogène et cylindrique. On obtient des résultats particulièrement simples si la grosseur du rayon laser est beaucoup plus petite que le diamètre des électrodes. La théorie se vérifie par rapport à l'espacement entre les électrodes, à la puissance et à la grosseur du rayon laser et à la fréquence de modulation; la meilleure sensibilité est obtenue avec une faible fréquence de modulation, une grande puissance du rayon laser et un faible espacement entre les électrodes. En autant que le rayon n'illumine pas la surface de l'électrode, le signal est indépendant de la grosseur du rayon laser. La précision des mesures est dominée par le bruit de fond dans le flot de courant à travers la résistance électrolytique. Opérant en solution aqueuse, avec un laser d'hélium-néon de 5-mW, on a obtenu des limites de détection de $5,5 \times 10^{-4}$ pour des mesures faites à travers des fils d'électrodes d'un diamètre de 76- μm . Avec cet instrument on peut facilement mesurer la différence d'absorbance de l'eau et de l'eau lourde, à 632,8 nm.

Mots clés : la modulation thermique de la conductivité électrique.

[Traduit par la revue]

Introduction

Photothermal techniques produce high sensitivity absorbance determination by measurement of the heat deposited within a sample following absorbance of light. This heat may be detected directly with a liquid helium cooled bolometer in molecular beam experiments (1) or the heat may be detected indirectly as a temperature rise with a thermocouple (2), as a pressure wave with a piezoelectric or microphonic transducer (3), as a variation in electron capture cross-section for gaseous samples (4), or as a refractive index disturbance with the variety of thermo-optical techniques (5). The latter class of thermo-optical techniques probably is the best developed analytical photothermal method for absorbance determination of liquid samples. In all cases, because the heat deposited within the sample following absorbance is directly proportional to the excitation energy, the absorbance of dilute and highly transparent materials may be measured by use of a high energy or high intensity light source.

Recently, we presented a preliminary report of a photothermal technique based upon the change in electrical conductivity with the temperature of an ionic solution (6). The principle of the measurement is rather simple. Small changes in the temperature of a volume of solution will result in relatively large changes in the viscosity of the solution because of the high thermal coefficient of viscosity for most liquids. The change in viscosity can be conveniently monitored by measuring the conductance of the solution because of the inverse relationship

between conductance and viscosity. In this paper, the conductance is measured by employing miniature, 76- μm diameter platinum electrodes that define the geometry for a small volume electrolytic resistor. A modulated laser beam intersects the electrolytic resistor. When an absorbing analyte is present and the beam is on, the temperature increases, causing a decrease in the viscosity of the solution and an increase in the current through the electrolytic resistor. When the beam is off, the solution cools and the current decreases. The current (or conductivity) signal can be demodulated at the chopping frequency of the laser by a lock-in amplifier. The amplitude of the demodulated signal is proportional to the absorbance of the solution whereas the phase is related to thermal diffusion within the sample.

Small volume absorbance measurements are of importance in a number of technological fields, including detection for the chromatographic and electrophoretic analysis of biological materials. Although a number of thermo-optical techniques have been developed for small volume absorbance determinations (7), the thermally modulated electrical conductivity (TMEC) technique appears to offer the greatest promise for analysis of aqueous samples.

Theory

The coordinate system used in the model is shown in Fig. 1. A laser beam, aligned along the Z axis of a Cartesian system, intersects the cylindrical electrolytic resistor centered on the X axis and defined by the radius of the electrode, r , and the

¹To whom correspondence should be addressed.

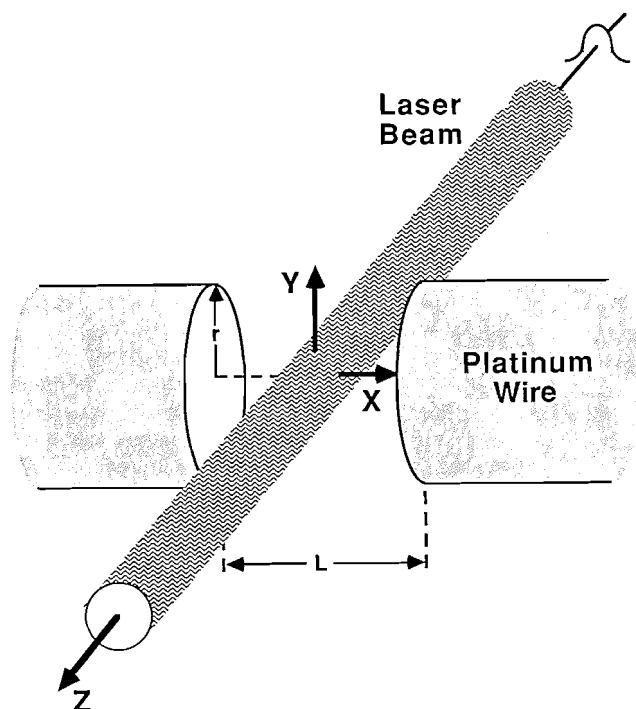


FIG. 1. Interaction of the beam with a cylindrical electrolytic resistor.

distance between the electrodes, L . Normally, the beam is aligned to intersect the center of the resistor. The change in current as a function of time following a pulse of light has been derived in Appendix 1. This impulse response function may be simplified greatly if the laser beam spot size is much smaller than the radius of the wire. In this case, the impulse function takes on a simple form

$$[1] \quad \Delta I_{\text{impulse}} \left[\begin{array}{c} \text{small spot} \\ \text{limit} \end{array} \right] = \frac{2.303E\epsilon CI}{\pi rL} \left[\frac{-1}{\rho C_p \eta} \frac{d\eta}{dT} \right]$$

where E is the energy of the laser pulse, ϵ is the molar absorptivity of the analyte, C is analyte concentration, and I is the average current passing through the resistor. The term in brackets is the solvent constant that is a function of the solvent density ρ , heat capacity C_p , viscosity η , and the derivative of the viscosity with respect to temperature $d\eta/dT$. The solvent constant, Table 1, changes by about a factor of three for the different solvents listed (5, 8–10). Interestingly, water has a solvent constant which is within a factor of two of the best solvent listed, ethanol. Of course, the low dielectric constant of most organic liquids presents difficulty in preparation of high ionic strength solutions required for high precision measurements.

The small spot size limit of the impulse response function is quite remarkable. The signal is predicted to be independent of time, undergoing no decay. Time independence results because the thermally modulated electrical conductivity signal is a function of the average temperature rise in the volume between the electrodes. A decay in the impulse signal will occur only when the thermal energy diffuses to the bulk solution or to some other heat sink. Assuming that the radius of the wire is less than the separation between the electrodes, the thermal decay is characterized by a diffusion time

$$[2] \quad t_{\text{diffusion}} \approx \frac{r^2}{D}$$

TABLE 1. Physical constants of solvents^a

Solvent	Density (g/mL)	Heat capacity (J/g °C)	Viscosity η (cP)	$d\eta/dT$ (cP/°C)	$10^3 \times$ Solvent constant ^b (mL/J)
Water	0.998	4.18	1.002	-0.0245	5.86
Methanol	0.791	2.46	0.597	-0.0076	6.54
Ethanol	0.789	2.36	1.200	-0.0232	10.4
Acetonitrile	0.786	2.17	0.360	-0.0030	4.89
Acetone	0.790	2.18	0.326	-0.0021	3.74

^aAll constants are at 20°C. Obtained from refs. 5, 8–10.

^bThe solvent constant = $(-\eta\rho C_p)^{-1} d\eta/dT$.

where the thermal diffusivity of the solution, D , is given by

$$[3] \quad D = \frac{k}{C_p \rho}$$

where k is the thermal conductivity of the solution. For time shorter than the diffusion time, no decay in the impulse signal is predicted. Also, the signal is predicted to be independent of the laser beam spot size. This observation is understandable, given the dependence of the signal on the thermal energy contained between the electrodes. The signal is predicted to be inversely related to the radius of the electrode, r , and the electrode spacing, L . The former observation arises because the average temperature rise of the solution will depend inversely upon the volume of the electrolytic resistor; an inverse second power dependence is not observed because the laser beam crosses perpendicular to the electrolytic resistor. Integration over the beam path results in the observed inverse first power dependence on the wire radius. The inverse dependence of the signal upon both the wire radius and the electrode spacing is important for application of this technique to small volume absorbance determinations; the signal increases as the sample volume decreases, essentially because the thermal energy is contained within a smaller sample volume.

To obtain the change in current passing through the electrode for an arbitrary excitation waveform, it is necessary to convolute the impulse response function with the appropriate excitation function. For example, the current response obtained at time t after the start of a step excitation by a light source of power P is simply given by

$$[4] \quad \Delta I_{\text{step}} \left[\begin{array}{c} \text{small spot} \\ \text{limit} \end{array} \right] = \frac{2.303P\epsilon CI}{\pi rL} \left[\frac{-1}{\rho C_p \eta} \frac{d\eta}{dT} \right] t$$

The current change is expected to increase linearly with time following illumination with a continuous wave light source. Again, the approximation will be valid for time less than $t_{\text{diffusion}}$.

Experimental

Figure 2 presents a block diagram of the cell used to characterize the technique. The electrodes were constructed by drawing glass tubing over 76- μm diameter platinum wire. The finished electrodes had an outer diameter of 530 (± 10) μm . The ends of the electrodes were polished progressively using coarse polishing cloth, 6 μm diamond polishing compound, 3 μm alumina, and finally 1 μm alumina. The cell was machined from a Teflon block with an inner chamber volume of ca. 0.3 mL. A "V" groove was cut across the front of the block in which the electrodes could sit to a depth such that they remained flush with the front face of the block. A quartz window presses firmly against the front of the block and is held in place by a thick Teflon ring. The laser beam enters the cell through the front window and

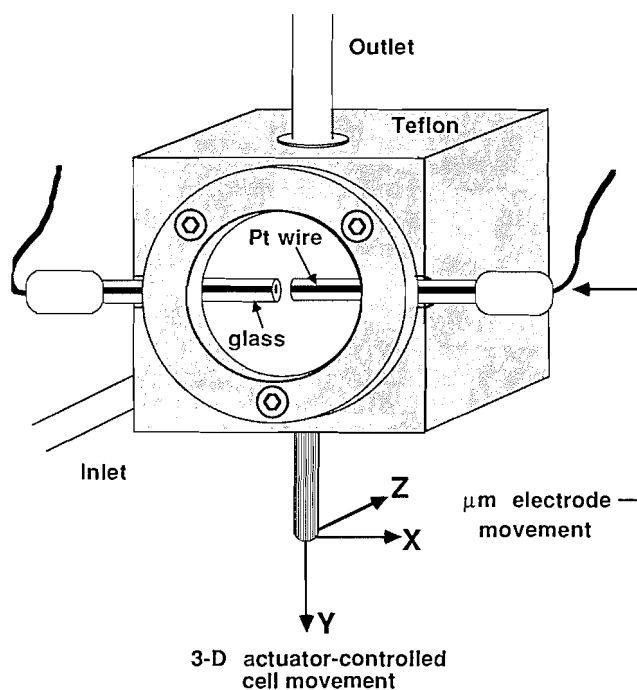


FIG. 2. Diagram of the cell used for characterization of TMEC.

exits through a second window at the back of the cell. The distance the beam travels in solution before it passes the electrode central axis is about $265\ \mu\text{m}$. One of the electrodes is held stationary while the other is driven along its axis using a translation stage-micrometer assembly. In this way the electrode spacing could be varied accurately while maintaining the platinum faces of the electrodes directly opposite each other in a parallel plate configuration. The entire cell-electrode assembly was mounted on translation stages for movement in three dimensions by computer controlled actuators.

The conductance of the solution between the electrodes is measured using an ac method. The electronics used are similar to those described previously (6). Briefly, a $40\ \text{kHz}$ frequency carrier wave is applied to the electrodes. The ac current passing through the cell is amplified, half-wave rectified and smoothed using a four pole low-pass active filter with $300\ \text{Hz}$ cutoff frequency. The resultant dc signal is linear with the conductivity of the solution for cell impedances of $>10\ \text{k}\Omega$; for typical solutions and electrode spacing, the cell impedance was greater than $100\ \text{k}\Omega$. It was found that, with the present electrode configuration, a carrier wave frequency of $40\ \text{kHz}$ was needed in order to minimize the impedance due to double layer capacitance; the system acts as a high pass filter with a cut-on frequency of about $10\ \text{kHz}$. In addition, there are three parallel capacitive impedances that should be made as large as possible in order to reduce any non-electrolytic current flow (11). They are (i) cell capacitance, (ii) contact and lead capacitance, and (iii) physical electrode capacitance (due to the parallel plate configuration). The cell capacitance was minimized by grounding the metal inlet and outlet ports of the cell. The contact and lead capacitance was reduced by careful construction. The physical electrode capacitance is dependent on the dielectric material and the electrode dimensions. In total, the current flow due to all three of these capacitances was typically $<10\%$ of the electrolytic current flow. This value would be unacceptable for an absolute conductance measurement but is quite acceptable for the differential measurement of conductance in this photothermal technique.

A block diagram of the experiment is presented in Fig. 3. A $5\ \text{mW}$, linearly polarized He-Ne laser beam ($632.8\ \text{nm}$) passes through an optical chopper. Mirrors are used to manipulate the beam through a 2-mm diameter aperture that acts to reduce stray light. A $10\times$, $16\ \text{mm}$ focal length lens focuses the beam to a small spot between the electrodes in the cell. The light exiting the cell strikes a photocell that generates a reference signal for the two-channel lock-in amplifier. The

conductivity circuit described above provides the signal for the lock-in amplifier. The lock-in measures both the amplitude and phase of the thermally modulated conductivity signal simultaneously.

For the purpose of beam positioning and for generating X-Y scans, an 855C Newport programmable controller and actuators were used to control the movements of the cell with respect to the laser beam. The controller is capable of $0.1\ \mu\text{m}$ movements although such resolution was not needed in this application. A computer was used to communicate with the controller and to store data from the lock-in as incremental movements were made.

Chemicals

Aqueous solutions were typically $0.01\ \text{M}$ NaCl. Fast Green FCF dye (Aldrich, 96%), which has a strong absorbance at the He-Ne wavelength, was used for the experiments without further purification. The visible spectrum of the dye was recorded in water as a function of its concentration, NaCl concentration, and pH with a HP 8451A diode array spectrophotometer. A $0.01\ \text{M}$ salt concentration was found not to have any effect on the spectrum. The dye behaves as an acid-base indicator, changing from violet in strongly alkaline solutions, to aqua in neutral solutions, to green in acidic solutions. The spectrum is relatively constant as the concentration of the dye is increased in neutral solutions up until about $10^{-5}\ \text{M}$. Above this concentration, the intensity of the main α band centered at $624\ \text{nm}$ starts to decrease in intensity. This decrease in intensity is not due to a change in pH that occurs as the dye concentration is increased but instead appears to be due to aggregation of the dye molecules (12).

Results and discussion

The cell-electrode arrangement was first characterized with respect to conductivity detection. For a $0.01\ \text{M}$ NaCl solution, the current through the cell was measured for various electrode separations. As expected, the current was found to be inversely proportional to the electrode separation ($R = 0.998$, $n = 15$) in the range of 40 to $3000\ \mu\text{m}$ at a constant applied voltage. A small positive intercept was observed in the data that is attributable to the parallel capacitances mentioned previously. The current through the cell was also found to be linear with the applied voltage ($R = 0.9991$, $n = 12$) in the range of 0 to $3\ \text{V rms}$. Above this voltage, resistive heating of the solution between the electrodes led to positive curvature. The upper limit to the voltage that may be applied to the electrodes is determined by the effects of resistive heating. Heating of the solution between the electrodes could result in convection currents, which would presumably lead to additional noise in the system; the current was found to be more stable over a long period of time with lower applied voltages. For this reason, voltages of less than $1\ \text{V rms}$ were used for most subsequent experiments.

Two sources of modulated electrical conductivity are expected: that due to absorbance of the sample and that associated with stray light which illuminates the electrodes. To characterize the latter signal, the thermally modulated electrical conductivity signal was measured as the laser beam was moved with respect to the cell. Figure 4 shows the lock-in amplitude as a function of position near the electrodes in the X-Y plane of Fig. 1, using a blank solution and a chopping frequency of $200\ \text{Hz}$. Individual pixels in the plot are $10\ \mu\text{m}$ on a side. An image of the wire is observed as two hills separated by a valley of weakly absorbing blank solution. The signal drops off quite quickly as the laser spot moves along the wire away from the resistor region. Because the resistance of the wire is negligible in comparison to that of the electrolytic resistor, it appears that the background signal associated with the illuminated wire arises as heat diffuses through the wire to the solution within the electrolytic resistor volume. As the laser beam illuminates

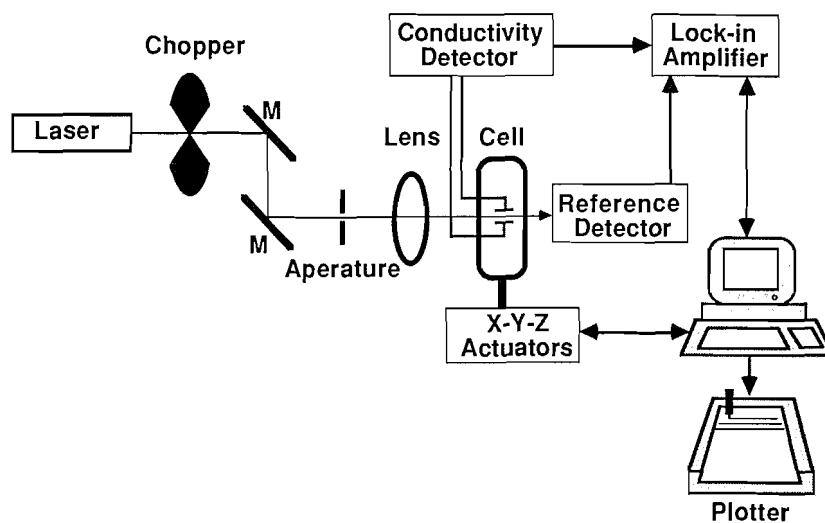


FIG. 3. Schematic diagram of the experiment.

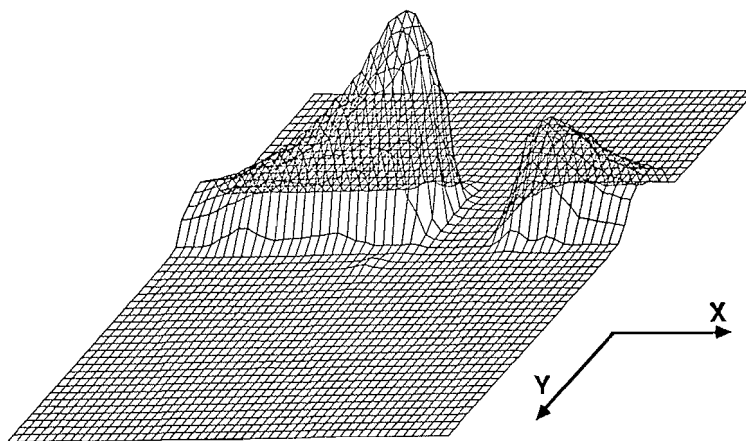


FIG. 4. A laser scan (X-Y) of the signal generated in the vicinity of the electrodes for a non-absorbing solution. The signal due to conductance of heat along the wire into the resistor region has generated a "picture" of the electrodes. TMEC absorbance measurements are made by aligning the beam to pass between the electrodes. Each pixel is $10\ \mu\text{m}$ on a side.

the wire at larger distances from the electrolytic resistor, less heat is transported to the solution during each chopper cycle and an exponential decrease in signal is observed.

Absorbance measurements of a sample are generated when the laser illuminates the valley region between the electrodes. Figure 5 shows three close-up scans of the region between the electrodes using step sizes of $2.5\ \mu\text{m}$. Figure 5a shows the scan using a blank solution. The edges of the wire are observable as sharp rises in signal on the left and right sides of the scan. Any residual signal on the valley floor constitutes a background signal for the absorbance measurement. The magnitude of the background signal has been greatly reduced in this study as compared to our preliminary report (6). This decreased background signal results from careful minimization of beam reflections from the windows, use of polished electrode surfaces, and use of platinum as an electrode metal, which has a lower absorption than many other metals including copper (8). Figures 5b and 5c show scans of the same region with a dye concentration in solution of $4.0 \times 10^{-5} M$ for chopping frequencies of 10 Hz and 200 Hz, respectively. The signal maximizes between the electrodes and then falls off gradually in the radial direction. This signal, generated when the laser is shining in the

region outside the resistor volume, is due to diffusion of heat into the resistor region. During the 50 ms illumination period during each chopping cycle, heat will diffuse approximately $100\ \mu\text{m}$ — similar to the distance over which an appreciable hump is observed in Fig. 5b. At a chopping frequency of 200 Hz, Fig. 5c, heat will travel about $20\ \mu\text{m}$ during the chopper cycle and little signal is generated in the solution outside of the electrolytic resistor.

With $20\ \mu\text{m}$ spatial resolution provided by the 200 Hz chopping frequency, the signal strength generated between the electrodes reflects the local sensitivity of the measurement and not the effects of heat flow. A dip in the signal between the electrodes along the X axis in Fig. 5c is not due to increased background signal at the electrodes, see Fig. 5a, but rather may arise from increased sensitivity near the electrodes. The origin of this increased sensitivity would be associated with the higher current density near the electrode face compared with the region in the center of the electrolytic resistor. To test this idea, the magnitude of the electric field along the axis between two parallel, circular electrodes is derived in Appendix 2. The magnitude of the electric field vector pointing along the electrode axis is given by

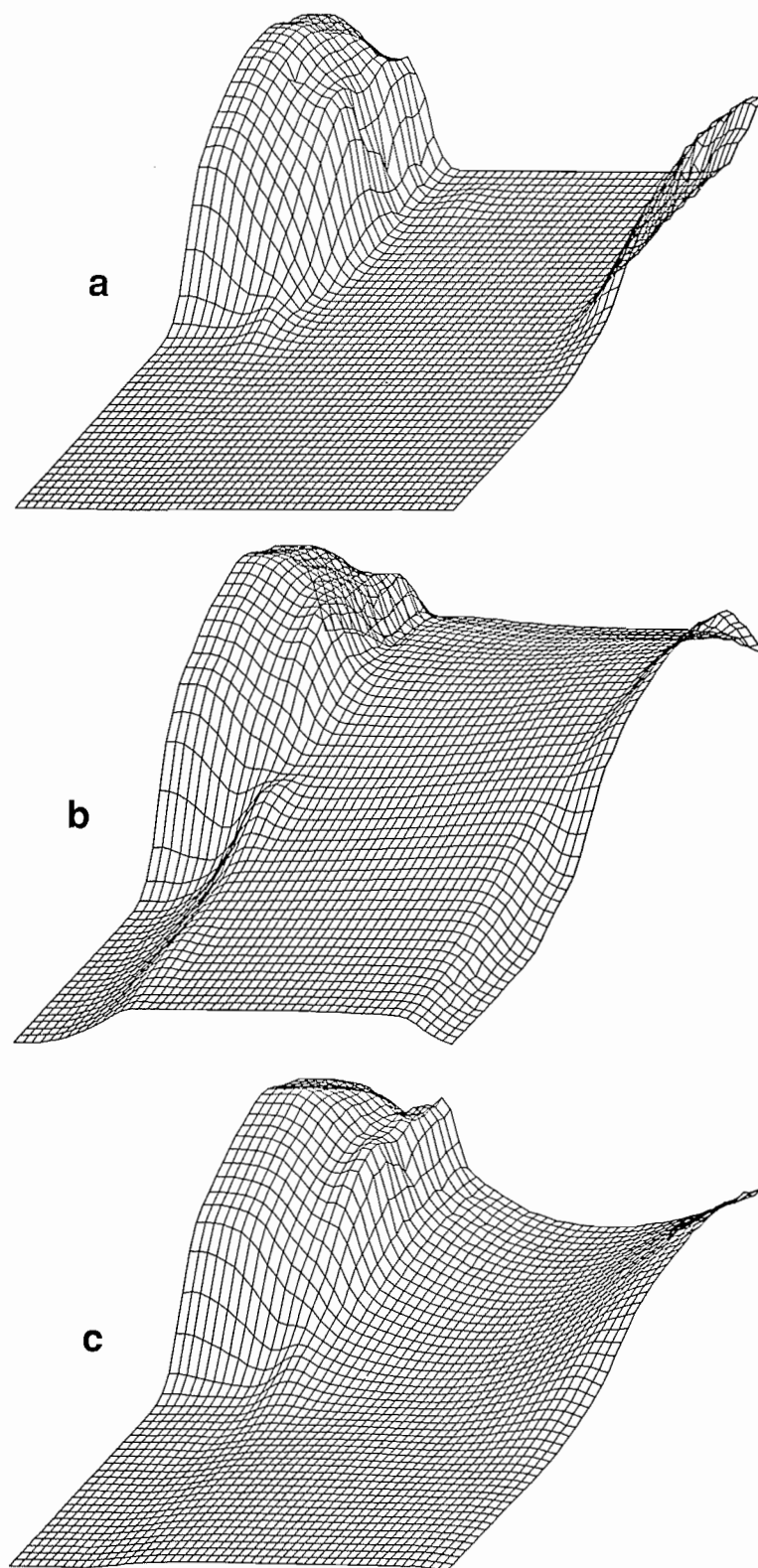


FIG. 5. Closeup scans (X-Y) of the signal in the resistor region using $2.5\ \mu\text{m}$ pixels: (a) blank solution in the cell; (b) strongly absorbing solution with a chopping frequency of 10 Hz; (c) strongly absorbing solution with a chopping frequency of 200 Hz. The variation of the magnitude of the electric fields along the resistor axis become apparent at this higher chopping frequency. A "U" shape results for the TMEC absorbance signal in the X direction between the electrodes.

$$[5] \quad E = \frac{\sigma}{K\epsilon_0} \left[1 - (1/2) \left(\left[\frac{1}{1 + \{R/(0.5 + \beta)\}^2} \right]^{1/2} + \left[\frac{1}{1 + \{R/(0.5 - \beta)\}^2} \right]^{1/2} \right) \right]$$

where K is the dielectric constant of the medium, ϵ_0 is the permittivity of free space, R is the ratio of the wire radius r to the electrode separation L , and β is the distance from the electrode face divided by the electrode separation. Equation [5] is plotted as a function of β for various values of the dimensionless parameter R in Fig. 6. As R approaches ∞ , corresponding to small electrode separations and large values of r , the electric field along the axis becomes uniform and approaches that given for a parallel plate configuration, $|E_{pp}| = \sigma/K\epsilon_0$ (13). The electric fields in the diagram are presented as a fraction of this value. As R decreases, the electric field along the axis of the resistor decreases: the magnitude of the field at the electrode surface asymptotically approaches a limit of $E_{pp}/2$ and the electric field at the center of the resistor approaches zero. The curve marked with squares has a R value of 0.381, corresponding to the particular $r:L$ ratio used for the data in Fig. 5. The shape of the squared line in Fig. 6 qualitatively matches the shape of the dip between the electrodes in Fig. 5c. Higher sensitivity is achieved near the electrode face due to the greater magnitude of the electric fields there. To quantitatively compare Figs. 5c and 6, it is necessary to integrate the non-uniform electric field strength with the volume of the laser beam.

With the laser beam focused at the center of the electrolytic resistor, with a 100 μm electrode spacing, and utilizing a weakly absorbing solution, the dc current and the lock-in signal were measured as the voltage was increased from 0.0 to 3.0 V rms. The lock-in signal was found to be linear with the current ($R = 0.9998$, $n = 12$) as predicted from the theory. For all other data, the voltage applied to the electrodes was held at 1.0 V.

A linear polarizer was used to vary the laser power and a power meter was used to measure the power of the beam at the entrance to the cell. Using an electrode spacing of 50 μm , the lock-in signal increased linearly with the power ($R = 0.9998$, $n = 7$). However, the noise was constant to the maximum power of 5 mW. This constant noise and linear dependence of signal on laser power suggests that increasing the power further will result in increased sensitivity and improved detection limits.

The noise in the system appears to be associated with the conductivity of the electrolytic resistor. In fact, the noise appears to be due to shot noise in the current passing through the resistor. The current fluctuation associated with shot noise is given by (14)

$$[6] \quad I_{\text{noise}}(\text{rms}) = (2eIB)^{1/2}$$

where e is the electron charge, I is the average current through the cell, and B is the bandwidth of the measurement. Typical ac currents through the cell are 2.5 μA rms and the frequency bandwidth of the lock-in is given by $(1/8)T_c$ using the time constant T_c . Taking amplification into account, the expected shot noise appearing at the lock-in was 0.5 μV . Depending on the day, the noise that was measured was anywhere from one to six times this fundamental limit for chopping frequencies of 10 to 100 Hz. Using a resistor of 300 k Ω in place of the cell resulted in noise that was consistently within a factor of two of the shot noise limit.

Sensitivity was measured as a function of the electrode spacing, L , and chopping frequency, f , under constant current con-

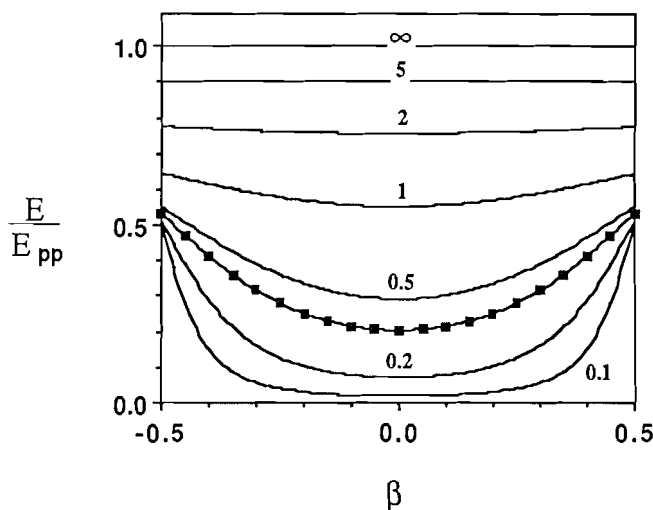


FIG. 6. Plotted are the calculated curves (eq. [11]) for the variation of the magnitude of the electric field on axis due inside a cylindrical parallel plate configuration. β is the fractional distance along the x axis between the electrodes and each curve represents a particular R value: the ratio of the wire radius to the electrode separation. E_{pp} is the field inside a parallel plate capacitor, achieved as R approaches infinity. The squared line represents the fields for an R ratio of 0.381, that used in the scans of Fig. 5.

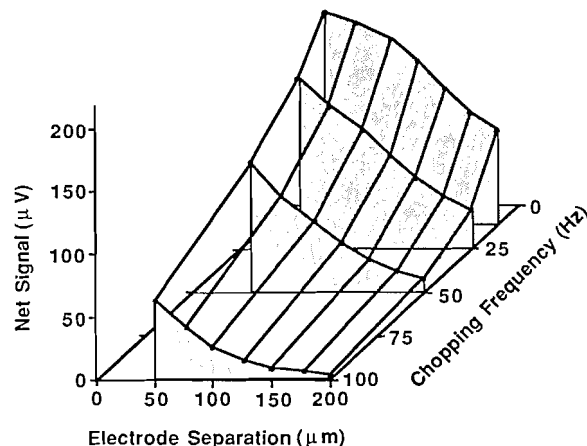


FIG. 7. Variation of the absorbance signal as a function of the electrode separation and chopping frequency. Greater sensitivity is achieved by using small electrode separations and low chopping frequencies.

ditions for the ranges $L = 50$ to $200 \mu\text{m}$ and $f = 10$ to 100 Hz. The results are shown graphically in Fig. 7. The signal increases with a decrease in the chopping frequency at all electrode separations; lower chopping frequencies allow more heat to be deposited within the electrolytic resistor during each chopping cycle and, hence, a larger modulated signal. Of course, the temperature can not increase without bound between the electrodes. Eventually, heat will diffuse to the electrodes or other heat sinks, limiting the maximum signal produced at low chopping frequency. The signal also increases with a decrease in the electrode spacing; a small volume solution will heat faster than a larger volume. Equations [1] and [4] predict that the signal is inversely proportional to the electrode spacing. However, as the electrodes come close together, heat flow to the electrodes will decrease the sensitivity of the measurement and light scatter onto the electrodes will increase the background

signal. In this instrument, the background signal increases when the electrode spacing is less than 50 μm . Highest sensitivity is produced at low chopping frequency and small electrode spacing.

To study the variation in signal with laser beam spot size, a relatively large electrode separation, 125 μm , was used to allow a wide range of spot sizes to be studied. The spot size was varied by moving the lens, which focuses the beam, with respect to the cell using a micrometer. The spot size of the beam between the electrodes was estimated by recording the background signal as the laser beam was moved from the solution onto the resistor. The background signal gave a good approximation to an error function for the overlap of the Gaussian beam with the electrodes and the spot size was estimated from this data. The signal observed when the laser beam was centered in the electrolytic resistor varied by less than two standard deviations as the laser beam spot size changed from 9 μm to 40 μm and at a chopping frequency of both 10 Hz and 50 Hz. Despite the fact that the spot sizes are relatively large, this spot size independence is as predicted from eqs. [1] and [4]. This independence of signal upon spot size is important because it suggests that relatively large beams from incoherent light sources could be used to generate the thermally modulated signal.

A calibration curve was generated with an electrode separation of 50 μm and a chopping frequency of 10 Hz for aqueous Fast Green dye ranging from $1.0 \times 10^{-8} \text{M}$ to $4.0 \times 10^{-5} \text{M}$ and 0.01 M NaCl. Two blank solutions were prepared; one in H_2O and the other in D_2O . The noise measured during the calibration was 3.6 times the shot noise limit. The calibration curve was linear ($R = 0.9998$, $n = 14$) over three orders of magnitude from the one point detection limit (3σ) of $6.9 \times 10^{-9} \text{M}$ to $1.0 \times 10^{-5} \text{M}$ dye concentration. At higher concentrations, the calibration curve shows negative deviation because of a change in the spectrum of the dye due to self-association and a decrease in the laser power reaching the electrodes due to absorbance of the beam through the 260 μm distance from the window to the electrodes.

The blank signal was not zero, even though the laser beam passed through the center of the electrolytic resistor. This background signal has two origins, one from light scatter on the electrodes and the other from the finite absorbance of H_2O at 632.8 nm. The effect of each contribution may be determined by comparing the background signal observed with 0.01 M NaCl in water and that observed with 0.01 M NaCl prepared in D_2O . Although the light scatter background for the two solvents should be similar, because the refractive index of the two solvents is similar, the absorbance of D_2O is much less than that of H_2O at 632.8 nm. The absorbance of water in the red portion of the spectrum is associated with overtones of infrared transitions; the higher mass of deuterium results in lower frequency infrared transitions and, hence, lower absorbance in the visible portion of the spectrum. The Fast Green - H_2O calibration line intercepts the D_2O blank signal level at a negative dye concentration of $-1.31 \times 10^{-8} \text{M}$. The absorbance of a positive amount of dye of this concentration should thus be interpreted as the difference in absorbance between H_2O and D_2O at a wavelength of 632.8 nm. The experimental value for this difference is $\Delta\epsilon C(\text{H}_2\text{O} - \text{D}_2\text{O}) = 1.3 \times 10^{-3} \text{cm}^{-1}$. The datum is in excellent agreement with the literature value of $1.22 \times 10^{-3} \text{cm}^{-1}$ determined using pulsed photoacoustic spectroscopy in a long path length cell (15).

The absorptivity-concentration product (ϵC) detection limit for the calibration was $7.2 \times 10^{-4} \text{cm}^{-1}$, made over a path

length given by the diameter of the wire, 76 μm . Using this path length, the absorbance detection limit is 5.5×10^{-6} , made in a volume of only 230 pL, estimated by the full resistor volume. The amount of analyte between the electrodes at the detection limit is only 1.6 attomoles or about a million molecules. Thermal modulation of electrical conductivity is a useful technique for the determination of absorbance within sub-nanoliter volumes of aqueous samples.

This excellent performance is achieved using a low power and low cost 5 mW laser. Of course, an increase in the laser power will result in a proportional increase in the sensitivity and decrease in the detection limit. For example, a 250-mW laser could produce detection limits on the order of 1×10^{-7} for aqueous samples, a significant advance in the state of the art. These detection limits are not likely to be exceeded with this particular cell geometry. Shot noise in the current flowing through the electrolytic resistor limits the precision of the conductivity technique. One approach to decrease the relative shot noise would be to increase the size of the electrodes which would increase the current through the increased electrolytic resistor. Unfortunately, the sensitivity of the measurements is predicted to scale inversely with the radius of the wire. Increasing the wire diameter will improve the precision of the measurement while decreasing the sensitivity of the measurement. It may prove necessary to investigate alternative cell geometries to improve further the performance of the technique.

Acknowledgements

This work was funded by the Natural Sciences and Engineering Research Council. The authors wish to thank Raymond Anthony Walford of the machine shop at the University of Alberta for his excellent work in construction of the Teflon cell. The software used for the collection of laser scans was developed by Messrs. Lee Tse Kheong and Dean S. Burgi.

1. T. E. GOUGH, R. E. MILLER, and G. SCOLES. *Appl. Phys. Lett.* **30**, 338 (1977).
2. G. H. BRILMYER and A. J. BARD. *Anal. Chem.* **52**, 685 (1980).
3. D. BETTERIDGE and P. J. MEYLOR. *CRC Crit. Rev. Anal. Chem.* **14**, 267 (1984).
4. N. J. DOVICH and R. A. KELLER. *Anal. Chem.* **55**, 543 (1983).
5. N. J. DOVICH. *CRC Crit. Rev. Anal. Chem.* **17**, 357 (1987).
6. R. McLAREN and N. J. DOVICH. *Anal. Chem.* **60**, 730 (1988).
7. N. J. DOVICH. *Prog. Anal. Spectrosc.* **11**, 179 (1988).
8. R. C. WEAST and M. J. ASTLE (*Editors*). *CRC handbook of chemistry and physics*. 63rd ed. Chemical Rubber Publishing Company, Boca Raton, Florida. 1982.
9. D. R. LIDE (*Editor*). *Journal of physical and chemical reference data*. Vol. 11. 1982.
10. D. R. LIDE (*Editor*). *Journal of physical and chemical reference data*. Vol. 13. 1984.
11. J. BRAUNSTEIN and G. D. ROBBINS. *J. Chem. Ed.* **48**, 52 (1971).
12. B. C. BURDETT. *In Aggregation processes in solution*. Edited by E. Wyn-Jones and J. Gormally. Elsevier Scientific Publishing Company, New York. 1983. p. 241.
13. A. F. KIP. *Fundamentals of electricity and magnetism*. 2nd ed. McGraw-Hill, New York. 1969.
14. P. HOROWITZ and W. HILL. *The art of electronics*. Cambridge University Press, Cambridge. 1980.
15. A. C. TAM and C. K. N. PATEL. *Appl. Opt.* **18**, 3348 (1979).
16. A. W. ADAMSON. *A textbook of physical chemistry*. 2nd ed. Academic Press, New York. 1979.
17. A. J. TWAROWSKI and D. S. KLIGER. *Chem. Phys.* **20**, 253 (1977).

Appendix 1

In this appendix, a derivation is presented for the change in the current through a cylindrical electrolytic resistor induced by a pulsed Gaussian laser beam. The derivation of the impulse response involves a description of the current through a thermally non-homogeneous resistor, the temperature field produced by the laser and, finally, the change in the current.

The current through a cylindrical homogeneous resistor can be derived by calculating the current density in the resistor due to the movement of ions. The ions have a particular ion mobility and are subjected to a force from the electric field present in the resistor (16). Ignoring the complications from ion-ion forces, the current is given by

$$[7] \quad I = \sum_i \frac{M_i N z_i^2 e^2 \pi r^2 V}{6 \pi \eta r_i L}$$

where M_i is the molarity of the i th ionic species, z_i is the ionic charge number, r_i is the radius of the ion, e is the electron charge, N is Avogadro's number, V is the voltage applied to the electrodes, η is the viscosity of the medium, r is the radius of the resistor, and L is its length. The summation is over the current carrying ionic species in the solution. The current through a thermally non-homogeneous resistor can be described by a weighted average of the current in small volume elements of the resistor

$$[8] \quad \bar{I} = \frac{\int_{\text{vol}} I(x, y, z) dx dy dz}{\int_{\text{vol}} dx dy dz}$$

where the integral is evaluated over the cylindrical resistor volume. With the assumption that only the viscosity changes with temperature and defining the resistor volume, $\text{vol} = \pi r^2 L$, the current is given by

$$[9] \quad \bar{I} = \sum_i \frac{M_i N z_i^2 e^2 V}{4 \pi r_i L^2} \int_{\text{vol}} \frac{1}{\eta(x, y, z)} dx dy dz$$

where $\eta(x, y, z)$ is the local viscosity of the solution at a point. Equation [9] converges to eq. [7] for a homogeneous viscosity between the electrodes. The thermally induced current change, ΔI , is then given by differentiating with respect to temperature. Over the small temperature rise induced by absorbance of the laser beam, the viscosity will be inversely proportional to the temperature of the solvent. Collecting variables and simplifying

$$[10] \quad \Delta I = \frac{\partial I}{\partial T} \times \Delta T = \frac{\bar{I}}{\text{vol}} \left(\frac{-1}{\eta} \frac{d\eta}{dT} \right) \int_{\text{vol}} \Delta T dx dy dz$$

The current change is proportional to the temperature rise, ΔT , integrated over the resistor volume. The temperature rise excited by a pulsed Gaussian TEM₀₀ laser within a homogeneous absorbing sample has been derived (17) and, in the coordinate system of Fig. 1, is given by

$$[11] \quad \Delta T_{\text{impulse}}(x, y, t) = \frac{2.303 E \epsilon C}{2 \pi k t_c (1 + 2t/t_c)} \times \exp \left[\frac{-2(x^2 + y^2)}{\omega^2 (1 + 2t/t_c)} \right]$$

where k is the thermal conductivity of the solvent, ω is the spot size of the beam, t is the time after the pulse, and t_c is the time constant of the solvent.

$$[12] \quad t_c = \frac{\omega^2 \rho C_p}{4k}$$

Here, ρ is the solvent density and C_p is its thermal capacity. The impulse response of the current, $\Delta I_{\text{impulse}}$, is then given by substituting eq. [11] into eq. [10].

Taking the resistor center as the origin, the overlap integral of the temperature field with the resistor of eq. [10] may be evaluated using rectangular coordinates

$$[13] \quad \int_{\text{vol}} \Delta T_{\text{impulse}} d\tau = \frac{2.303 E \epsilon C}{2 \pi k t_c (1 + 2t/t_c)} \int_{-r}^r \int_{-\sqrt{r^2 - Z^2}}^{\sqrt{r^2 - Z^2}} \int_{-L/2}^{L/2} \exp \left[\frac{-2(X^2/\omega^2)}{(1 + 2t/t_c)} \right] \exp \left[\frac{-2(Y^2/\omega^2)}{(1 + 2t/t_c)} \right] dX dY dZ$$

The integration with respect to x is separable and yields an error function

$$[14] \quad \int_{-L/2}^{+L/2} \exp \left[\frac{-2x^2}{\omega^2 (1 + 2t/t_c)} \right] dx = \left[\frac{\pi \omega^2 (1 + 2t/t_c)}{2} \right]^{1/2} \text{erf} \left(\left[\frac{L^2}{2 \omega^2 (1 + 2t/t_c)} \right]^{1/2} \right)$$

The remaining integrals can not be expressed in terms of simple functions. Instead, we make the approximation that the spot size of the laser beam is much less than the radius of the wire. Under this condition, the limits of integration in the Y direction, become $\pm \infty$

$$[15] \quad \int_{\text{vol}} \Delta T_{\text{impulse}} d\tau = \frac{2.303 E \epsilon C \omega}{2 \sqrt{2 \pi} k t_c \sqrt{(1 + 2t/t_c)}} \times \text{erf} \left(\left[\frac{L^2}{2 \omega^2 (1 + 2t/t_c)} \right]^{1/2} \right) \times \int_{-r}^r \int_{-\infty}^{\infty} \exp \left[\frac{-2(Y^2/\omega^2)}{(1 + 2t/t_c)} \right] dY dZ = \frac{2.303 E \epsilon C r}{\rho C_p} \text{erf} \left(\left[\frac{L^2}{2 \omega^2 (1 + 2t/t_c)} \right]^{1/2} \right)$$

Collecting all together, the modulated current is given by

$$[16] \quad \Delta I = \frac{2.303 E \epsilon C \bar{I}}{\pi r L} \left(\frac{-1}{\rho C_p \eta} \frac{d\eta}{dT} \right) \times \text{erf} \left(\left[\frac{L^2}{2 \omega^2 (1 + 2t/t_c)} \right]^{1/2} \right)$$

Last, if the laser beam spot size is much less than the electrode spacing, the current is found to be

$$[17] \quad \Delta I_{\text{impulse}} \left[\begin{matrix} \text{small spot} \\ \text{limit} \end{matrix} \right] = \frac{2.303 E \epsilon C \bar{I}}{\pi r L} \left(\frac{-1}{\rho C_p \eta} \frac{d\eta}{dT} \right)$$

Assumptions

Various approximations have been made in the derivation of the impulse response of eq. [17]. These are listed below:

(i) The ions and absorbing analyte are homogeneously distributed between the electrodes.

(ii) In the derivation of the current of eq. [1], Stokes approximation has been invoked for the frictional coefficient of a spherical particle of radius r_i particle moving through a viscous medium: $f = 6\pi\eta r_i$ (16).

(iii) The electric field between the electrodes is of magnitude

$$E = V/L \text{ — inside the cylindrical resistor volume} \\ (V = \text{applied voltage})$$

$$E = 0 \text{ — elsewhere}$$

This approximation will hold in the limit of small electrode spacing. An accurate model would account for the variation in electric field strength throughout the sample volume. Appendix 2 presents the variation in the axial electric field between the electrodes. A uniform axial electric field is achieved if the radius of the wire is more than five times the distance between the electrodes.

(iv) The voltage drop across the double layer capacitance is assumed to be zero. This is achieved by using a sufficiently high ac frequency to eliminate the double layer impedance.

(v) The spot size of the laser is assumed constant over the diameter of the electrolytic resistor.

(vi) The effects of heat sinks such as quartz windows and platinum wires have been ignored.

(vii) The background signal associated with scattered light striking the electrodes is ignored.

(viii) The modulation frequency of the conductivity measurement is sufficiently low so that eq. [7] holds.

Appendix 2

This appendix presents a derivation for the magnitude of the electric field at a point on the axis of a cylindrical parallel plate capacitor. The calculation involves summing all the contributions to the field at point P to all charge on the surface of the electrode faces as shown in Fig. 8.

A charge density $+\sigma$ exists on the left electrode surface and an equal and opposite charge density exists on the right electrode surface. An incremental electric field vector, dE , at point P is calculated from Coulombs law (13)

$$[18] \quad dE = \frac{1}{4\pi K\epsilon_0} \frac{dq}{l^2} l$$

where dq is the element of surface charge a distance l away from point P and l is a vector pointing along the line from the surface charge to point P. When calculating the field on axis

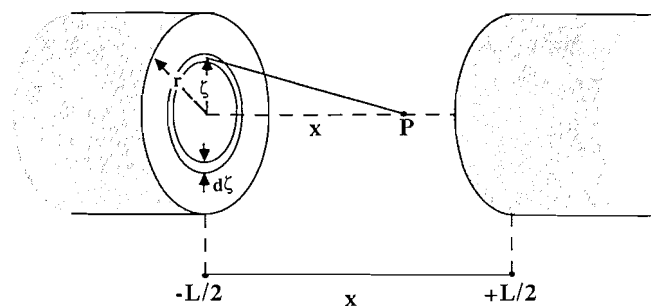


FIG. 8. Calculation of the magnitude of the electric fields on axis due to cylindrical parallel plate configuration. X is distance measured from the center of the electrode.

due to a thin circular ring of surface charge on an electrode face, the vector components perpendicular to the x axis can be ignored due to cancellation by symmetry. Thus, the field at P due to a charged ring of radius ζ and thickness $d\zeta$ on the left electrode face is given by

$$[19] \quad dE = \frac{1}{4\pi K\epsilon_0} \frac{2\pi\zeta d\zeta \sigma}{[(L/2 + x)^2 + \zeta^2]} \frac{(L/2 + x)}{\sqrt{(L/2 + x)^2 + \zeta^2}} x \\ = \frac{(L/2 + x)\sigma}{2K\epsilon_0} \frac{\zeta d\zeta}{[(L/2 + x)^2 + \zeta^2]^{3/2}} x$$

The total field at point P due to the left electrode is obtained by integrating with respect to ζ

$$[20] \quad dE_{\text{LEFT}} = \frac{(L/2 + x)\sigma x}{2K\epsilon_0} \int_0^r \frac{\zeta}{((L/2 + x)^2 + \zeta^2)^{3/2}} d\zeta$$

Substituting $y = \zeta^2$, the integral yields

$$[21] \quad E_{\text{LEFT}} = \frac{\sigma x}{2K\epsilon_0} \left(1 - \left[\frac{1}{1 + \{r/(L/2 + x)\}^2} \right]^{1/2} \right)$$

The field at P due to charge on the right electrode can be calculated in a similar fashion and will add to the field calculated above. It is convenient to use the fractional distance between the electrodes; $\beta = x/L$ and to calculate the field for a particular ratio of the wire radius r to the electrode separation L ; $R = r/L$. The final expression for the magnitude of the field at P using these substitutions is

$$[22] \quad E(\beta, R) = \frac{\sigma}{K\epsilon_0} \left[1 - (1/2) \left(\left[\frac{1}{1 + \{R/(0.5 + \beta)\}^2} \right]^{1/2} \right. \right. \\ \left. \left. + \left[\frac{1}{1 + \{R/(0.5 - \beta)\}^2} \right]^{1/2} \right) \right]$$